Sensors and Actuators A 293 (2019) 62–69

Contents lists available at ScienceDirect

Sensors and Actuators A: Physical

journal homepage: www.elsevier.com/locate/sna

Geometric correction for TanSat atmospheric carbon dioxide grating spectrometer

Hang Zhang, Yuquan Zheng, Shuai Li, Chao Lin, Chengliang Li, Jingze Yuan*, Yue Li*

Changchun Institute of Optics, Fine Mechanics and Physics, Chinese Academy of Sciences, Changchun, 130033, China

ARTICLE INFO

Article history:
Received 20 January 2019
Received in revised form 1 April 2019
Accepted 22 April 2019
Available online 23 April 2019

Keywords:
Geometric correction
Centroid position
Deflection error

ABSTRACT

Carbon Observing Satellite (TanSat) is the first of Chinese experimental satellite for monitoring the CO2 column densities in the atmospheric, while identifying sources and sinks on regions scales. Three grating spectrometers are equipped on TanSat to measure the reflected sunlight in the 0.76μm O2A-band, 1.61μm weak CO2 band and 2.06μm strong CO2 band respectively. Three bands have high spectral resolution and signal to noise ratio (SNR), while their spectral and radiometric calibration have been reported in many articles. This paper describes the geometric calibration of the essential payload (ACGS) on the TanSat. In the assembly process, the flatness only in the spatial dimension is strictly controlled owing to the physical obstruction. The geometric deflection error in one band should be tested and corrected by adjusting the starting rows of different spectral samplings. Meanwhile, the alignment error among the three bands also need processing in the same way to ensure that the slits of the three bands were matched the corresponding geographic target. Finally, the geometric correction results of the thermal-vacuum testing suggested that the alignment accuracy is well enough to match the requirements.

1. Introduction

Atmospheric CO2 is the dominant component in anthropogenic greenhouse gas and plays an important role in climate change. In recent years, a lots of countries have paid more attention on space-based remote sensing for atmospheric CO2 concentrations. Compared with traditional ground-based observing sites, the technology of space-based remote sensing has more ability to worldwidely acquire the distribution and discharge information on regional scales, with high speed and repeatability. The two most representative instruments on orbit are the Japanese GreenHouse Gases Observing Satellite (GOSAT) and NASA Orbiting Carbon Observatory-2 (OCO-2). They were launched on January 23, 2009 and July 2, 2014, respectively, and since then, have provided a huge amount of global atmospheric CO2 observational data to help research the global carbon cycle [1–4].

TanSat is the third satellite aiming to measure global atmospheric CO2 concentrations from space, which is supported by the Ministry of Science and Technology of the China Earth Observation Program. TanSat was launched into the 705 km sun-synchronous orbit on December 22, 2016, with an inclination angle of 98.75°. The two payloads on TanSat are the Atmospheric Carbon dioxide Grating Spectrometer (ACGS) and Cloud & Aerosol Polarimetric Imager (CAPI) [5–7]. The ACGS provides the space-based measurements to quantify terrestrial sources and sinks of CO2 with a high accuracy. The CAPI is used to identify the contamination by optically-thick clouds and to minimize the impact of scattering created by aerosol.

As the ACGS is the main payload on TanSat, this paper focuses on the geometric offset and correction of the ACGS and is organized as follows: Section 2 describes a review of the instrument and the main performance requirements. Section 3 presents the test of geometric offset and correction method. Section 4 provides the results of geometrical matching. The final section gives a conclusion of this work.

2. Instrument overview

2.1. Design of ACGS

As shown in Fig. 1, the ACGS consists of a telescope, a collimating system, a large-area plane diffraction grating, and a spectral imaging system, possessing three spectral bands: 0.76 μm-O2A band, 1.61 μm weak CO2 band and 2.06 μm strong CO2 band. The most important component of the grating spectrometer is the diffraction grating. The size of each grating is 140 mm × 190 mm and the diffractive efficiency can be over 90% [8,9]. At the focus of each spec-

* Corresponding authors.
E-mail addresses: zhanghang_ciomp@sina.com (H. Zhang), yuanjz@ciomp.ac.cn (J. Yuan), liyue_ciomp@sina.com (Y. Li).

https://doi.org/10.1016/j.sna.2019.04.034
0924-4247/

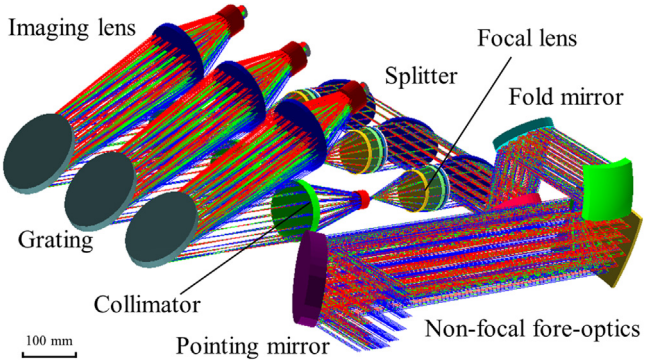

Fig. 1. Optical layout of the ACGS.

trometer for the corresponding spectral band, hyperspectral image is recorded by an area array detector. One dimension is used to measure the different wavelengths as the spectral dimension, while the other is used to detect the field of view along the entrance slit as the spatial dimension [10–12]. For the 0.76 μm band, the silicon detector 55-30 from E2V Technologies Corporation is chosen, 320 pixels are used out of the total 576 in the spatial dimension and 1200 pixels are used in the spectral dimension. In the spatial dimension, 16 pixels are merged into one footprint [13]. For the 1.61 μm and 2.06 μm band, the HgCdTe detector (Sofradir Company) consisting of a 500(spectral dimension) ×256(spatial dimension) pixels array is adopt. Regarding 500 pixels in spectral dimension, all of them are treated as spectral channel. Meanwhile, in the spatial dimension, 240 pixels are selected from the total 256. And then, sets of 12 are averaged to yield 20 spatial footprints. The ACGS has a spatial resolution of 2 km × 2 km, a swath of 20 km. Depending on whether the spatial pixels are merged or not, there are two modes (the merging mode and the full frame mode) for the output spectral images created by the focus plane array (FPA) [14,15].

2.2. Spectral and radiometric performance

The ACGS is a precision instrument for measuring the solar radiation reflected by the earth-atmosphere system quantitatively. High spectral and radiometric resolution is the prerequisite to retrieve CO2 concentration accurately. Table 1 shows a summary of the ACGS spectral and radiometric performance [16,17]. Increasing the spectral resolution can improve the instrument sensitivity to detect the content of CO2. Nevertheless, the SNR of each channel will decline. The pixels in the spatial dimension are combined to increase the SNR. According to the Nyquist Theorem, there must be over 2 spectral samples to obtain complete spectral information, that is, there are more than two detector elements per full width at half maximum (FWHM) in the spectral dimension for each band [18,19].

2.3. Geometric calibration

The ACGS is a quantitative instrument with high precision, while many articles have reported its spectral and radiometric calibration [20–22]. However, the geometric calibration of the ACGS has barely been reported.

The ACGS consists of three imaging spectrometers. To match the data inversion requirements, three spectrometers need to disperse the same geographic position into the spectrum at the same time. Meanwhile, a given geographic position after spectral dispersion should image onto a single row of pixels on the FPA. In other words, spatial overlap factor $c_{i,j}$ of any two spectral sampling pixel in one band should be higher than 0.9. The function $c_{i,j}$ is defined as below:

$$c_{i,j} = 1 - \iint \left| \frac{r_i(x,y)}{2k_i} - \frac{r_j(x,y)}{2k_j} \right| dxdy \quad (1)$$

where $r_n(x, y)$ is the contour of the two dimensional, scan smeared spatial response for the n th spectral sample, and k_n is a normalizing constant given by the equation:

$$k_n = \iint r_n(x,y)dxdy \quad (2)$$

$c_{i,j}$ of 1(100%) corresponds to a perfect bore sight alignment; $c_{i,j}$ of 0 corresponds to zero spatial overlap in the co-sampled scenes. As defined, $c_{i,j}$ includes effects due to spatial response nonuniformity among spectral samples, spatial misalignment of spectral samples, and timing errors of spatial misalignments due to scanning and/or spacecraft motion.

In order to fulfil the above geometric requirement, the spectrometer slit, the grooves on the diffraction grating, and columns of the detector need tightly aligning to ensure that a fixed series of rows on the FPA will sample the same angular field of view throughout the spectral range recorded by the FPA. In the instrument assembly process, the spectrometer slit and the grating grooves were unable to strictly parallel. As a result, the actual spectrum plane expressed as a parallelogram on the coordinate system of the FPA (spectral dimension and spatial dimension). The rectangular detector was used to sample the actual spectrum plane, thus the parallel of only one dimension could be realized. In the initial alignment process, we didn't attach much importance on the seriousness of deflection error in the spectral dimension, while the flatness only in the spatial dimension was strictly controlled. Therefore, the beginning row index for each spectral sample channel needed adjusting to compensate this deflection error. Geometric correction accuracy requirement: deflection errors in one band is under 1.6 pixels, and deflection errors among the three bands are under 2.5 pixels.

3. Geometric deflection testing

As mentioned above, the spectral image of one geographic point was not parallel to the rows of the detector. Therefore, geometric deflection error in one band needed testing and correcting. Meanwhile, the alignment error among the three bands should be processed samely to ensure that the slits of the three bands can match the same geographic target. Measuring the absolute spatial positions of the three spectrometer slits is the prerequisite to correct the alignment error among the three bands.

Table 1
Summary of the ACGS spectral and radiometric performance.

	O2A band	WCO2 band	SCO2 band
Central wavelength (nm)	760	1610	2060
Spectral range(nm)	758-778	1594-1624	2041-2081
Spectral resolution(nm)	0.033-0.047	0.12-0.15	0.16-0.2
SNR	360:1@5.8 × 10^{19}photons/sec/m^2/sr/μm)	240:1@2.1 × 10^{19}photons/sec/m^2/sr/μm)	180:1@1.1 × 10^{19}photons/sec/m^2/sr/μm)
Spectral sampling	2.0-2.8 pixels per slit	2.0-2.3 pixels per slit	2.0-2.7 pixels per slit

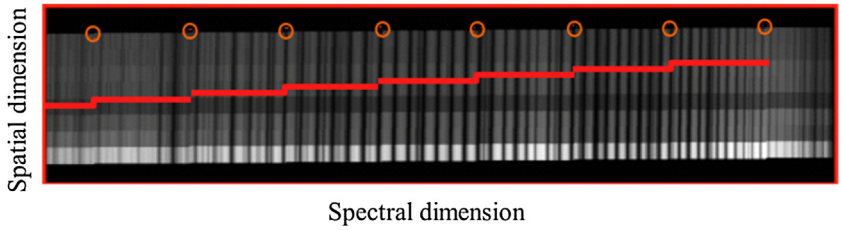

Fig. 2. Diagram of the deflection error in one band for the full frame mode, the abscissa is the spectral dimension and the ordinate is the spatial dimension.

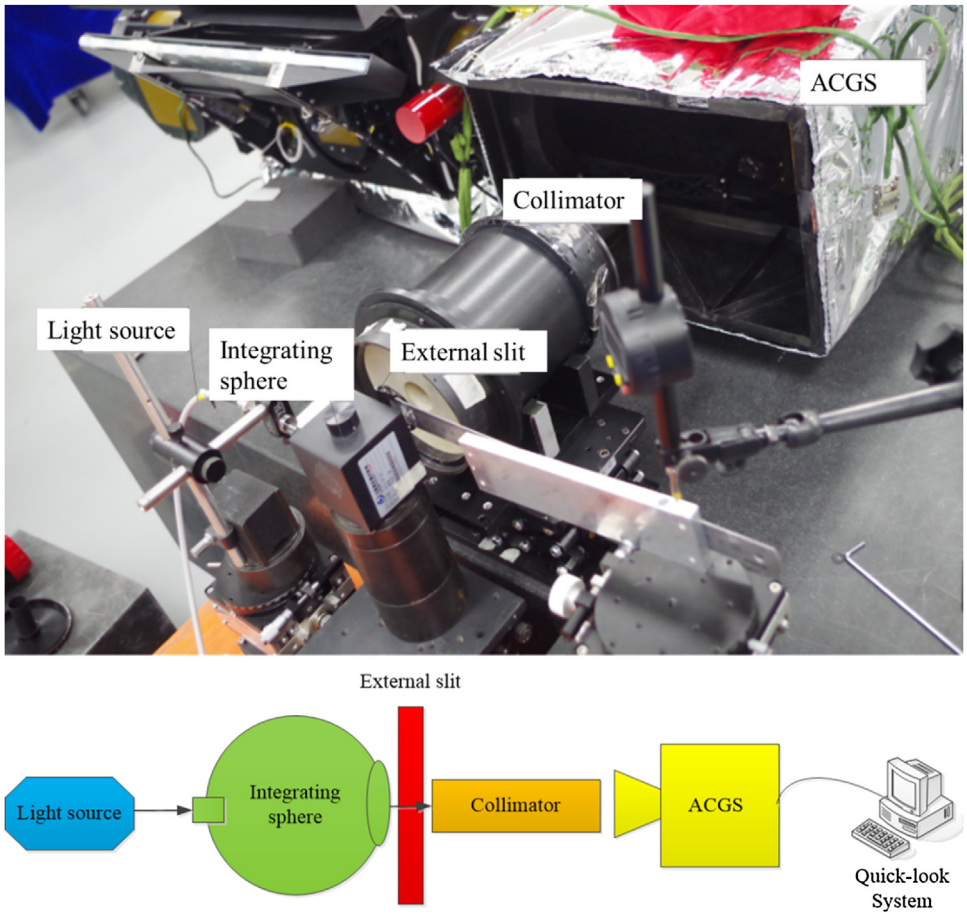

Fig. 3. Layout of the deflection error testing system in one band.

3.1. Deflection error in one band

The diagram of the deflection error is shown in Fig. 2. For a single spectrometer, one point of the slit was illuminated. After spectral dispersing, the slit was imaged on the different spectral pixels of the FPA. In the full frame mode, each spectral channel was imaged on different spatial position (row index) of the FPA. This is the main reason causes the spatial aliasing in the merging mode. It is meant that different spectral channel is not identical to the corresponding geographic position.

Firstly, the deflection error in one band was tested. Fig. 3 shows the experimental device. The light from the laser source was introduced into a 2 inch diameter integrating sphere by optical fiber. An external slit (was different from the slit of the ACGS) was illuminated to form an approximate line light source (20 μm width) [23]. The light passed through the collimator and entered into the ACGS. The external slit was focused onto the focal plane of the fore-optics of the instrument via the telescope system and the dichotic splitter. That is, the intersection between the instrument slit and the image of the external slit was illuminated [24]. Three bright lines along the spectral dimension were formed on the FPAs of the three spectrometers. Image centroid deviation of the spatial dimension sampled by different spectral channel represented the deflection error in one band.

Fig. 4 shows the original images and the centroid positions of the spatial dimension for the 0.76 μm, 1.61 μm and 2.06 μm band.

(b) The original image of the deflection error test and centroid slope of the spatial dimension based on the narrow line for the 1.61 μm band. Channel 1 = 89.94, channel 500 = 92.53. The red line is the linear regression result of the 1.61 μm band.

(c) The original image of the deflection error test and centroid slope of the spatial dimension based on the narrow line for the 2.06 μm band. Channel 1 = 94.3, channel 500 = 96.2. The red line is the linear regression result of the 1.61 μm band.

According to the results above, the deflection errors in the band for the 0.76 μm, 1.61 μm and 2.06 μm bands are 10.25 pixels, 2.59 pixels and 1.9 pixels, respectively.

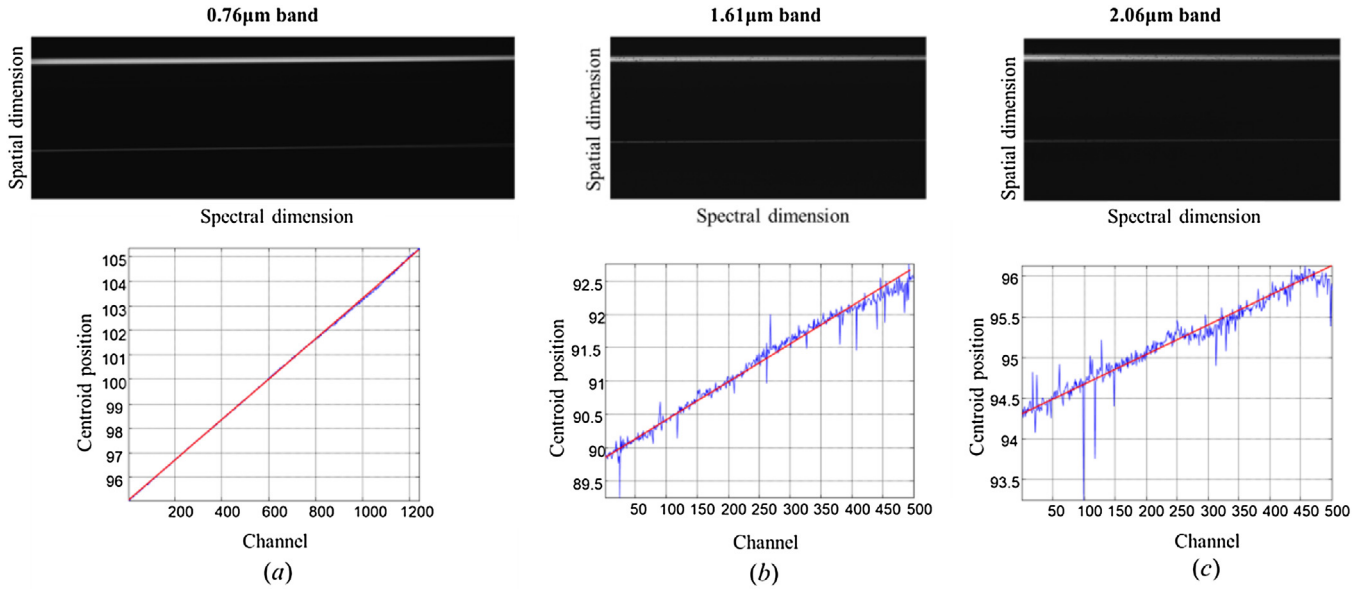

Fig. 4. (a) The original image of the deflection error test and centroid slope of the spatial dimension based on the narrow line for the 0.76 μm band. Centroid position varies with spectral channel, the abscissa is the spectral channel index, and the ordinate is spatial position of the centroid, channel 1 = 95.07, channel 1240 = 105.32. The red line is the linear regression result of the 0.76 μm band (For interpretation of the references to colour in this figure legend, the reader is referred to the web version of this article).

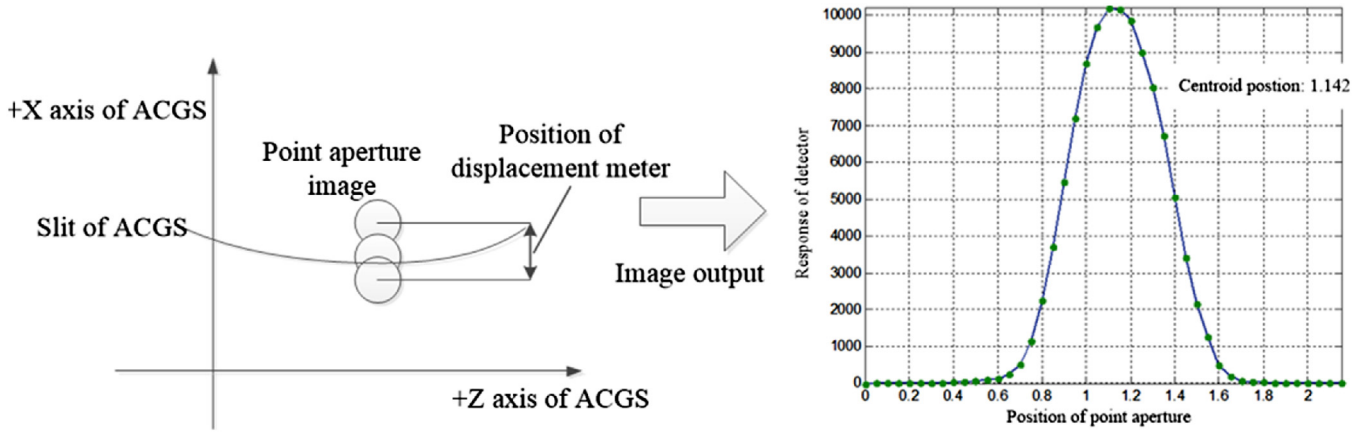

Fig. 5. The schematic diagram of the test for absolute spatial positions of the three spectrometer slits.

3.2. Test for absolute spatial positions of the three spectrometer slits

The test for absolute spatial positions of the slits was conducted in laboratory. A 0.3 mm point aperture was placed on the focus of the collimator with a 3 m focal length. The full aperture of the ACGS was illuminated. According to the focal length ratio, the size of the 0.3 mm point aperture imaged on the ACGS slit was 0.025 mm. The point aperture was moved up and down, and a displacement meter was adopted to measure the moving amount. The maximum response of the detector was obtained with peak searching [25]. The absolute spatial positions of the three spectrometer slits were acquired. The schematic diagram of the test is shown in Fig. 5.

The results of the test are shown in Fig. 6. The abscissa represents the horizontal spatial position of the slit, one side of the slit for the 1.61 μm band is regarded as the zero point. The ordinate represents the vertical position of the slit.

During the test, the starting row index for the 0.76 μm band was the 130th row, for the 1.61 μm band was the 7th row, for the 2.06 μm band was the 5th row. The test results are summarized in Table 2.

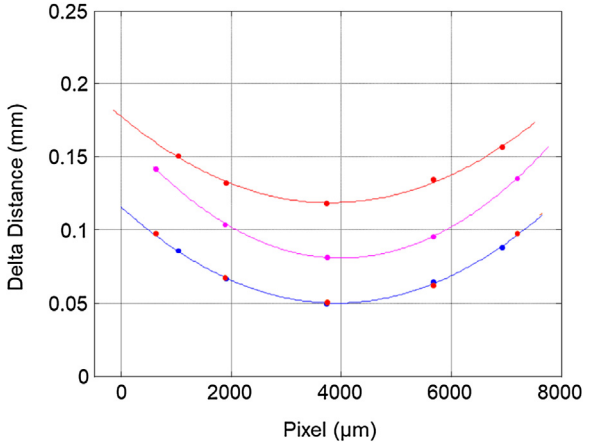

Fig. 6. The results of the test for spatial position of the three spectrometer slits. The red line (top), the purple line (middle) and the blue line (bottom) represents the 2.06 μm band, the 0.76 μm band and the 1.61 μm band, respectively. (For interpretation of the references to colour in this figure legend, the reader is referred to the web version of this article).

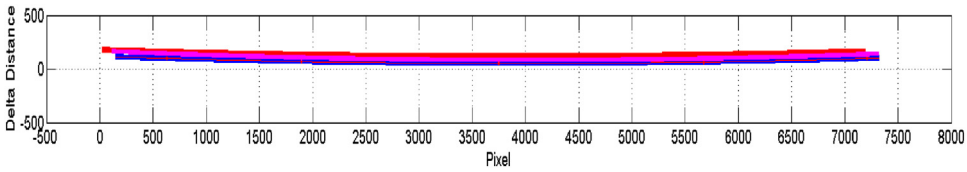

Fig. 7. The results of the test for spatial position of the three spectrometer slits (the x coordinate and y coordinate have the identical scale).

Table 2
The spatial positions of the spectrometer slits.

Spectral band	Horizontal position of initial pixel	Average relative vertical position (taking 1610 nm band as the benchmark)
760nm	588.9μm	0.0363 mm
1610 nm	210μm	0mm
2060nm	81.2μm	0.06735mm

Table 3
The starting pixel of each segment interval for the 0.76 μm band.

The initial pixel of 1 st segment	2nd	3rd	4th	5th	6th	7th	8th	9th	10th	11th
1	122	243	364	485	606	727	848	969	1090	1211

Table 4
The starting pixel of each segment interval for the 1.61 μm band.

The initial pixel of 1 st segment	2nd	3rd
1	194	388

The x coordinate and y coordinate are set to the same scale, as shown in Fig. 7. The results show that the three spectrometer slits are in well consistency.

3.3. Geometric correction method

According to the test results of deflection error in one band and spatial positions of the three slits, it was decided that the pixel integration mode need adjusting to correct the geometric offset. That is, the starting row index for different spectral channel should be adjusted. 0.76μm band

The deflection value in the 0.76 μm band was 10.25 pixels (full frame mode). Therefore, we divided the spectral dimension of the FPA into 11 segments, we kept the first segment as it was, while the starting row indexes of the rest 10 segments were adjusted in increments of one pixel successively. Segment interval M is calculated according to the formula below:

$$M = \frac{1pixel}{10.25/1242} = 121pixel$$

The starting pixel of each segment interval is given in Table 3.

1.61μm band:

The deflection value in the 1.61 μm band was 2.59 pixels (full frame mode). Therefore, we divided the spectral dimension of the FPA into 3 segments, we kept the first segment as it was, while the starting row indexes of the rest 2 segments were adjusted in increments of one pixel successively. Segment interval M is calculated according to the formula below:

$$M = \frac{1pixel}{2.59/500} = 193pixel$$

Table 5
The starting pixel of each segment interval for the 2.06 μm band.

The initial pixel of 1 st segment	The initial pixel of 2nd segment
1	264

The starting pixel of each segment interval is given in Table 4.

2.06 μm band:

The deflection value in the 2.06 μm band was 1.9 pixels (full frame mode). Therefore, we divided the spectral dimension of the FPA into 2 segments, we kept the first segment as it was, while the starting row index of the other segment was adjusted in increments of one pixel. Segment interval M is calculated according to the formula below:

$$M = \frac{1pixel}{1.9/500} = 263pixel$$

The starting pixel of each segment interval is given in Table 5.

4. Result validation

For confirming the effect of deflection correction, the ACGS was placed in the thermal-vacuum chamber to conduct geometric matching test after correction. The external slit (the identical slit mentioned in Section 3.1) was located on the focus of the collimator with a 3 m focal length. The three spectrometer slits of the ACGS were illuminated in the full aperture, the image data was stored by the quick-look system. Fig. 8 shows the layout of the geometric matching testing system.

The 1.61 μm band and 2.06 μm band of the ACGS could directly output the full frame image after geometric matching. Figs. 9 and 10 are the full frame images of the 1.61 μm and 2.06 μm band for the identical slit and the centroid position of the slit.

For the 0.76 μm band, the full frame image after geometric matching could not output because of the limit of storage capacity, however, the merging image could output. For validating the effect of geometric correction, the following method was used to obtain the full frame image. The width of the external slit was adjusted to less than 16pixel (full frame mode) of the FPA, and these pixels were just in one merging pixel, which was denoted by fov_n, while the adjacent pixel was denoted by fov_{n+1}. After geometric matching, the starting row was increased from 1 to 16 pixels, the image data of the merging mode was stored correspondently. Finally, the starting row was added to 16 pixels, that is, the merging pixel fov_n became the one fov_{n+1}. The starting row was set to a in the initial stage [26].

After geometric matching:

The 1 st row of full frame image of the external slit:

$$Line1 = fov_n(a) - fov_n(a+1)$$

The 2nd row of full frame image of the external slit:

$$Line2 = fov_n(a+1) - fov_n(a+2)$$

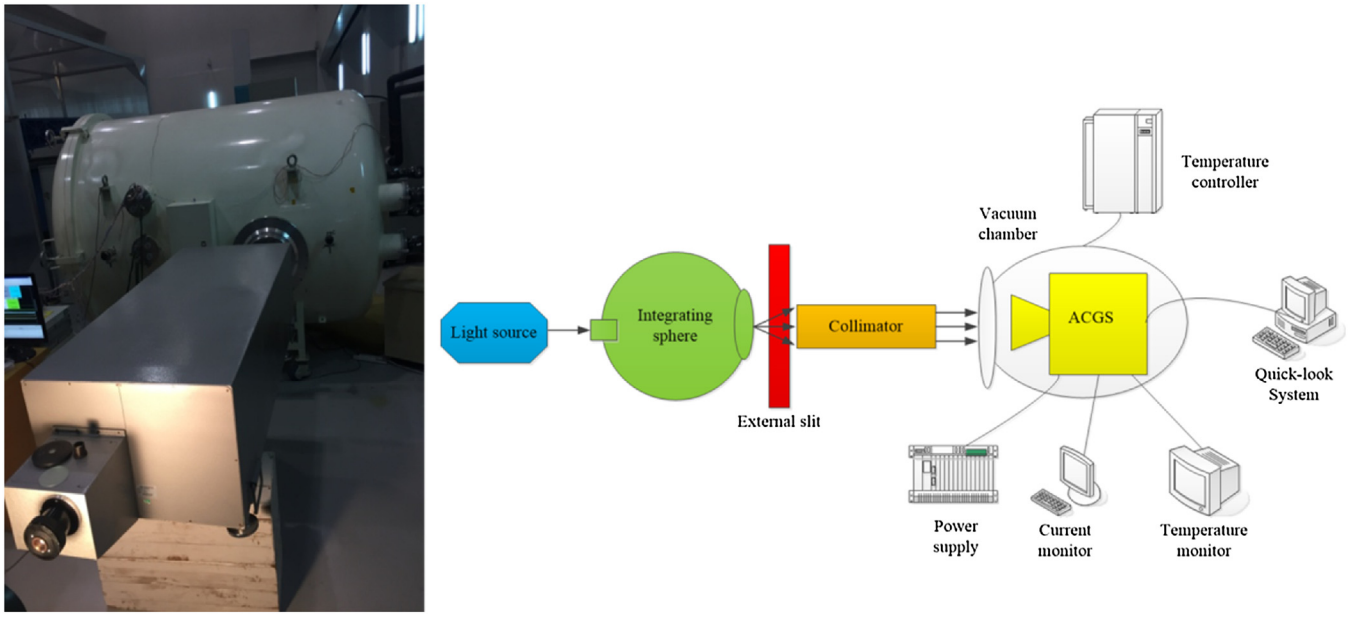

Fig. 8. The layout of the geometric matching testing system.

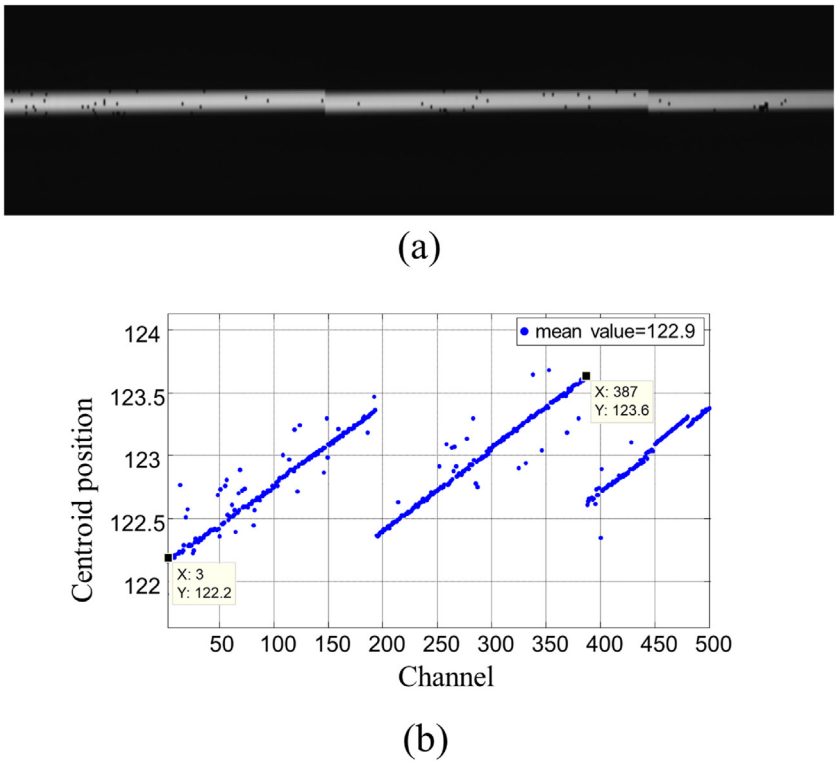

Fig. 9. (a) The full frame images of the 1.61 μm band for the identical slit after geometric matching. (b) The centroid position of the slit measured by the 1.61 μm band spectrometer, the maximum deviation is 1.4pixels.

The 16th row of full frame image of the external slit:

$$Line16 = fov_n(a+15) - fov_n(a+16) = fov_n(a+15) - fov_{n+1}(a)$$

The full frame image of the slit for the 0.76 μm band was obtained by using the method above, the image data is shown in Fig. 11.

The centroid positions of the slit measured by the three spectrometers are set to the same scale, as shown in Fig. 12. The average value of the alignment error among the three bands is 0.7pixel and the maximum value is 2pixels, matching the alignment accuracy requirements.

5. Conclusion

This paper reviewed the instrument design of ACGS firstly, and gave the spectral and radiometric performance parameters. The geometric deflection in one band and the alignment errors among the three bands, resulting from the physical obstruction in the

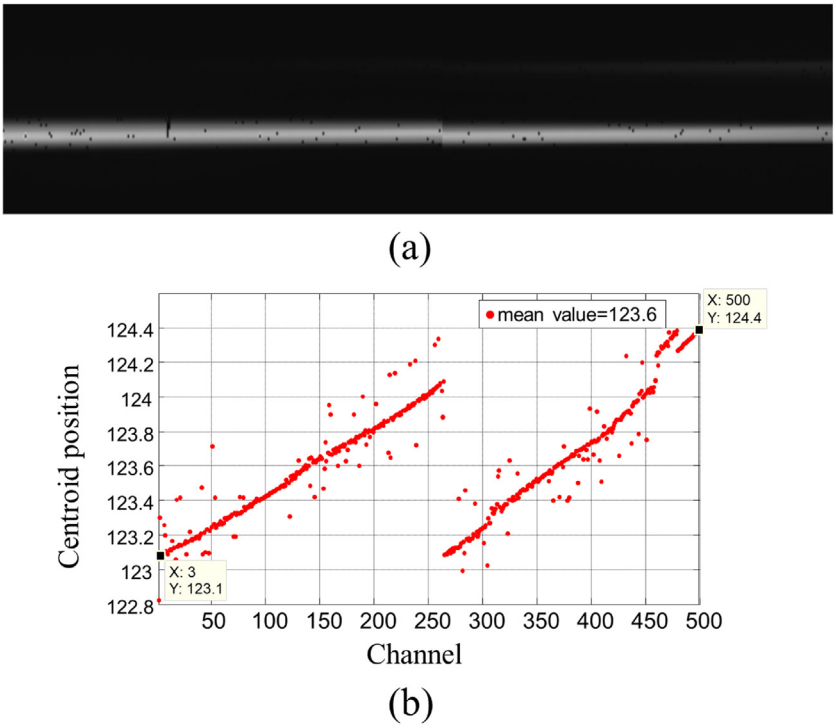

Fig. 10. (a) The full frame images of the 2.06 μm band for the identical slit after geometric matching. (b) The centroid position of the slit measured by the 2.06 μm band spectrometer, the maximum deviation is 1.3pixels.

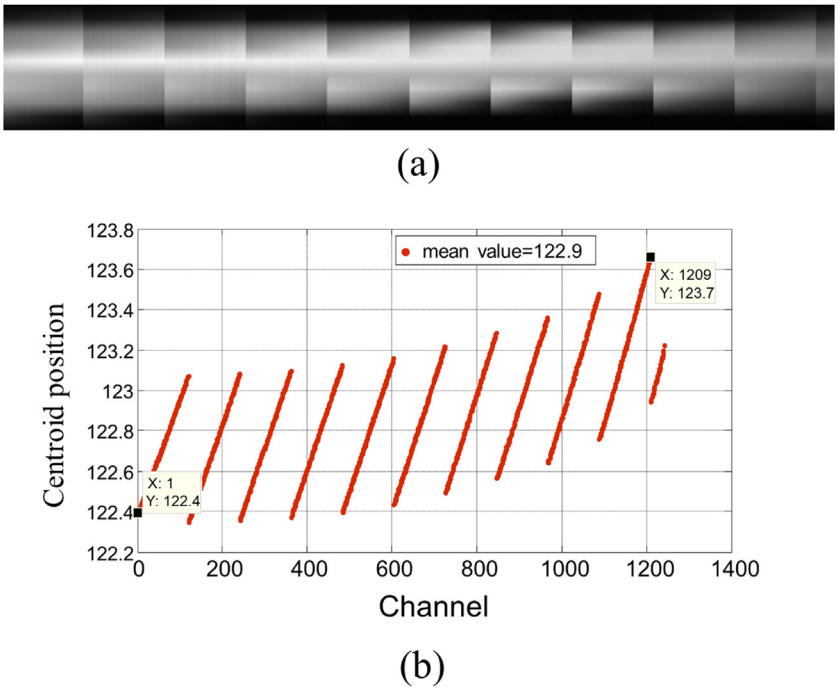

Fig. 11. (a) The full frame images of the 0.76 μm band for the identical slit after geometric matching. (b) The centroid position of the slit measured by the 0.76 μm band spectrometer, the maximum deviation is 1.3pixels.

instrument assembly process, were described emphatically. Using the point light illumination, three bright lines along the spectral dimension were imaged on the FPAs of the three spectrometers. The centroid position curves of the spatial dimension were measured, and the geometric offset in one band was observed. Then, the absolute spatial positions of the three spectrometer slits were measured. The geometric deflection was corrected by adjusting the starting rows of different spectral samplings. Finally, the geometric correction results were confirmed by thermal-vacuum testing. After processes above, the alignment accuracy are satisfactory to match the requirements

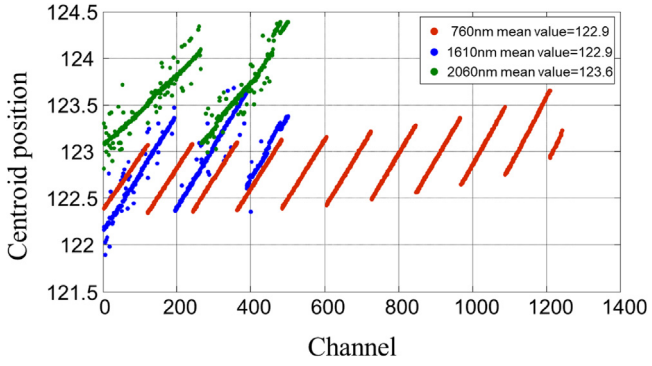

Fig. 12. The centroid positions of the slit that measured by the three spectrometers. Red line represents the 0.76 μm band, blue line represents the 1.61 μm band, and green line represents the 2.06 μm band (For interpretation of the references to colour in this figure legend, the reader is referred to the web version of this article).

Acknowledgments

The authors would like to thank every member of Carbon Observing Satellite science team, their contribution and kind support are necessary for this paper. This study was supported by the National Key Research and Development Program of China under Grants 2016YFB0500300.

References

[1] A. Kuze, T. Urbe, H. Suto, T. Hamazaki, The instrumentation and the BBM test results of thermal and near infrared sensor for carbon observation (TANSO) on GOSAT, Proc. SPIE. Int. Soc. Opt. Eng. 6297 (2006), 62970K.
[2] R.R. Basilio, H.R. Pollock, S.L. Hunyadi-Lay, OCO-2 (orbiting carbon observatory-2) mission operations planning and initial operations experiences, Proc. SPIE. Int. Soc. Opt. Eng. 9241 (2014), 924105.
[3] J.O. Day, C.W. O'Dell, R. Pollock, C.J. Bruegge, Preflight spectral calibration of the orbiting carbon observatory, Ieee Trans. Geosci. Remote. Sens. 49 (7) (2011) 2793–2801.
[4] C.W. O'Dell, J.O. Day, R. Pollock, C.J. Bruegge, D.M. O'Brien, Preflight radiometric calibration of the orbiting carbon observatory, Ieee Trans. Geosci. Remote. Sens. 49 (6) (2011) 2438–2447.
[5] H. Zhang, C. Lin, Y. Zheng, et al., Development and characterization of carbon observing satallite, J. Appl. Remote Sens. 10 (2) (2016), 024003.
[6] X. Chen, D. Yang, Z. Cai, Y. Liu, R.J.D. Spurr, Aerosol retrieval sensitivity and error analysis for the cloud and aerosol polarimetric imager on board TanSat the effect of multi-angle measurement, Remote Sens. (Basel) 9 (2017) 183.
[7] B. Yang, C. Yan, J. Zhang, X. Ju, Polarimetric calibration of multi-channel polarimetric imager, Opt. Precis. Eng. 25 (5) (2017) 1126–1134.
[8] P. Cu-Nguyen, A. Grewe, P. Feber, A. Seifert, S. Sinzinger, H. Zappe, An imaging spectrometer employing tunable hyperchromatic microlenses, Light: Sci. Appl. (2016) 5.
[9] Y. Wei, C. Lin, H. Xue, Y. Zheng, Design of mirror subassembly in CO2 sounder, Opt. Precis. Eng. 25 (3) (2017) 641–647.
[10] W. Luo, Y. Zhang, A. Feizi, Z. Gorocs, A. Ozcan, Pixel super-resolution using wavelength scanning, Light: Sci. Appl. 5 (2016), e16060.
[11] T. Zhang, G. Jin, C. Liu, Optical system design of multi-angle coupled framing camera, Chin. Opt. 11 (4) (2018) 615–622.
[12] D. Cao, G. Lin, X. Yang, Z. Zhang, B. Wen, Structure design and wavelength accuracy analysis of ultraviolet double grating spectrometer, Chin. Opt. 11 (2) (2018) 219–230.
[13] Z. Chang, Y. Wang, F. Si, H. Zhou, Digital binning method for CCD pixels and its applications, Opt. Precis. Eng. 25 (8) (2017) 2204–2211.
[14] F. Yue, C. Zhang, X. Zang, D. Wen, B.D. Gerardot, S. Zhang, X. Chen, High-resolution grayscale image hidden in a laser beam, Light: Sci. Appl. 7 (2018) 17129.
[15] B. Fazio, P. Artoni, M.A. Iati, Strongly enhanced light trapping in a two-dimensional silicon nanowire random fractal array, Light: Sci. Appl. (2016) 5.
[16] C. Lin, C. Li, L. Wang, Y. Bi, Y. Zheng, Preflight spectral calibration of hyperspectral carbon dioxide spectrometer of TanSat, Opt. Precis. Eng. 25 (8) (2017) 2064–2075.
[17] J. Mao, Y. Wang, E. Shi, Z. Zhang, F. Jiang, Spectral calibration based on echelle, Chin. Opt. 10 (3) (2017) 376–382.
[18] Z. Ii, C. Lin, Chengliang Li, L. Wang, Z. Ji, Prelaunch spectral calibration of a carbon dioxide spectrometer, Meas. Sci. Technol. 28 (2017), 065801.
[19] L. Zhang, T. Yue, J.P. Wilson, D. Wang, N. Zhao, Modelling of XCO2 surfaces based on flight tests of TanSat instruments, Sensors 16 (2016) 1818.
[20] Z. Yang, Y. Zheng, Z. Yin, C. Lin, Y. Bi, Laboratory spectral calibration of the TanSat atmospheric carbon dioxide grating spectrometer, Geosci. Instrum. Methods Data Syst. Discuss. (2018) 1–12.
[21] Z. Yang, Y. Zheng, Z. Yin, C. Lin, Y. Bi, Laboratory radiometric calibration of the TanSat atmospheric carbon dioxide grating spectrometer, IEEE Trans. Geosci. Remote. Sens. 56 (7) (2018) 4225–4233.
[22] H. Zhang, Y. Zheng, C. Lin, W. Wang, Q. Wang, S. Li, Laboratory spectral calibration of TanSat and the influence of multiplex merging of pixels, Int. J. Remote Sens. 38 (13) (2017) 3800–3816.
[23] F. Li, Z. Li, X.Wang J. Wang, C. Lin, Self-calibrated spectral radiance standard source, Opt. Precis. Eng. 25 (8) (2017) 2004–2010.
[24] M. Wei, F. Xing, Z. You, A real-time detection and positioning method for small and weak targets using a 1D morphology-based approach in 2D images, Light: Sci. Appl. 7 (2018) 18006.
[25] M. Liu, J. Deng, X. Feng, F. Qian, Design of highly sensitive space point target detection system, Chin. Opt. 11 (1) (2018) 115–122.
[26] Q. Wang, J. Liang, Z. Liang, J. Lv, W. Wang, Y. Qin, Design of decentered aperture-divided optical system of infrared polarization imager, Chin. Opt. 11 (1) (2018) 92–99.

Biographies

Hang Zhang received the Ph.D. degree in physics from Jilin University, Changchun, China, in 2017. He is an associate researcher at the Changchun Institute of Optics, Fine Mechanics and Physics, Chinese Academy of Sciences (CAS). His research is focused mainly on the hyperspectral imaging and performance calibration of optical remote sensing instruments. He is a Member of Carbon Observing Satellite science team.

Yuquan Zheng received the Ph.D. degree in optical engineering from the Changchun Institute of Optics, Fine Mechanics and Physics, Chinese Academy of Sciences (CAS), Changchun, China, in 2000. He is a senior researcher of Carbon Observing Satellite science team. His research is focused mainly on hyperspectral imaging, design of optical system and laboratory calibration.

Shuai Li is currently pursuing the Ph.D. degree in optical engineering from the Changchun Institute of Optics, Fine Mechanics and Physics, Chinese Academy of Sciences (CAS), Changchun, China. His research concerns the laboratory calibration of hyperspectral spectrometer.

Chao Lin received the M.S. degree in mechanical engineering from Jilin University, Changchun, China, in 2009. He is an associate researcher at the Changchun Institute of Optics, Fine Mechanics and Physics, Chinese Academy of Sciences (CAS). His research interests include mechanical design and calibration of hyperspectral imaging instruments.

Chengliang Li is currently pursuing the Ph.D. degree in optical engineering from the Changchun Institute of Optics, Fine Mechanics and Physics, Chinese Academy of Sciences (CAS), Changchun, China. His research concerns the data processing of the laboratory calibration.

Jingze Yuan received the Ph.D. degree in optical engineering from the Changchun Institute of Optics, Fine Mechanics and Physics, Chinese Academy of Sciences (CAS), Changchun, China, in 2017. Her research is focused mainly on the optical design.

Yue Li received the Ph.D. degree in physics from Jilin University, Changchun, China, in 2012. He is an associate researcher at the Changchun Institute of Optics, Fine Mechanics and Physics, Chinese Academy of Sciences (CAS). His research is focused mainly on the optical engineering.